A Combined Study on Shock Diffraction

Mark Kenneth Quinn
Konstantinos Kontis

Aero-Physics Laboratory
University of Manchester
George Begg Building
Sackville Street
Manchester
UK
M13 9PL
mark.quinn-2@postgrad.manchester.ac.uk

Abstract

Shock wave diffraction is a complex process which has been studied at great length but has never been fully understood. The diffraction process creates numerous complex wave structures, a shear layer and a strong vortex. The structure of this shear layer has been the subject of numerous studies. Some simulations have shown this shear layer to be unstable, observing that it develops Kelvin-Helmholtz-style instabilities. Simulation performed in this work show a strong grid dependency. The diffraction process is widely regarded as self-similar in time; however, these instabilities have never been seen experimentally at small time scales. The high speed and small scale of the phenomena present make them extremely challenging to visualise using any experimental method. The aim of this work is to provide a complete picture of the phenomena that occur when a Mach 1.46 shock diffracts around a 172 degree corner while presenting the experimental techniques which are most suited to this type of flow.

Key words: shock tube, shock diffraction, CFD, PIV, shadowgraph

Introduction

When a travelling normal shock wave encounters an increase in area, it diffracts into the area increase. Skews [1] showed how the shock wave diffracts around different angles. He showed that past a critical angle of $75°$, the flow remains unchanged. As the shock wave diffracts around the corner, a contact surface is created. This surface separates the gas that has passed through the normal shock from that which has passed through the curved shock. If the induced flow cannot navigate the sharp corner, separation occurs leading to a shear layer which is swept into the strong vortex generated [2].

Figure 1 shows the flow features behind a weak shock diffracting around a sharp corner. For incident shock Mach numbers lower than $M_i = 1.8$, the flow features resemble those seen in Figure 1. Different regions of the flow are numbered (0-3') depending on which features they have been affected by. Flow that has been affected by the planar incident shock, I, is separated from the flow exposed to the curved shock by the contact surface, CS. The shear layer, SL, created as the flow cannot navigate the sharp corner, rolls up into the strong vortex, V. As the shock Mach number increases, the expansion wave train, ET, grows to become one large area of supersonic flow, culminating in a terminating shock.
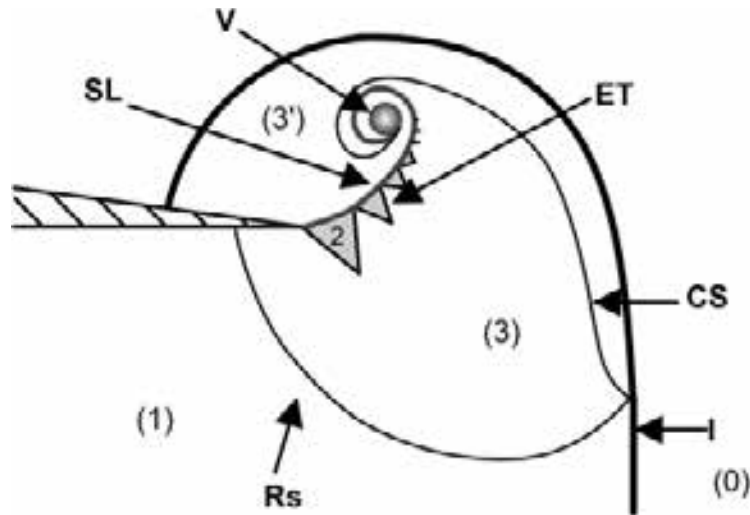
Figure 1. Weak shock diffraction Mi≈1.4

During the 18th International Symposium on Shock Waves, a special poster session was held to compare numerical codes from various researchers on the problem of shock diffraction [3]. The numerical results all showed the same strong features similar to those described above. Some of the codes showed that the shear layer was unstable and began to develop Kelvin-Helmholtz style instabilities. A later investigation into the problem by Sun and Takayama [4] found that solving the Euler equations gave an unstable shear layer, while solving the Navier-Stokes equation gave an undisturbed shear layer. As experimental evidence supporting the existence of the K-H instabilities was lacking, the authors assumed that the phenomenon was non-physical and attempted to suppress it by introducing more numerical diffusion into the simulations. Other researchers have found the shear layer in question to be stable or unstable, depending on the numerical resolution and exact formulation of the simulation [5-6].

Skews et al. [7-8] did manage to experimentally resolve some instabilities in the shear layer albeit at a significantly longer timescale than is required in simulations. This led them to conclude that the shear layer evolution process is not self-similar in time, as these instabilities have never been seen at small scales. The authors proposed that the upstream boundary layer characteristics could be a defining factor in the formation of the instabilities. However, inviscid simulations, notably by De & Thangadurai [5], captured the instabilities very clearly using inviscid simulations, leading to the doubts about the significance of the incoming boundary in the formation of this instability. Clearly this is an unsolved problem and is therefore deserving of further investigation. In this paper we will show simulations and experiments of a M_i=1.46 shock wave diffracting around a 172 degree corner.

Numerical Simulations

Numerical simulations were performed using the commercial CFD code Fluent as part of Ansys 13. A grid dependency study and solver discretisation study were both performed in order to determine the effect of numerics on the results. The grid is initialized at atmospheric pressure everywhere, with pressure outlet conditions at edges of the test sections including a sponge layer to avoid wave reflections. The driver section is then patched at the required pressure to generate the desired speed of shock wave based on inviscid theory.

Figure 2 shows the simulation of a whole shock tube (M_i=1.55) using 1st, 2nd, and 3rd order discretisation of both space and time and a comparison with inviscid theory. There appears to be little advantage to using a 3rd order solver, as the performance is almost identical in the region of shocks. The non-physical oscillations seen in the region of the diaphragm cast doubt about the robustness of the 3rd order solvers available in this code and their ability to deal with the wide range of phenomena present. For this reason, both 2nd order space and time discretisation was chosen.
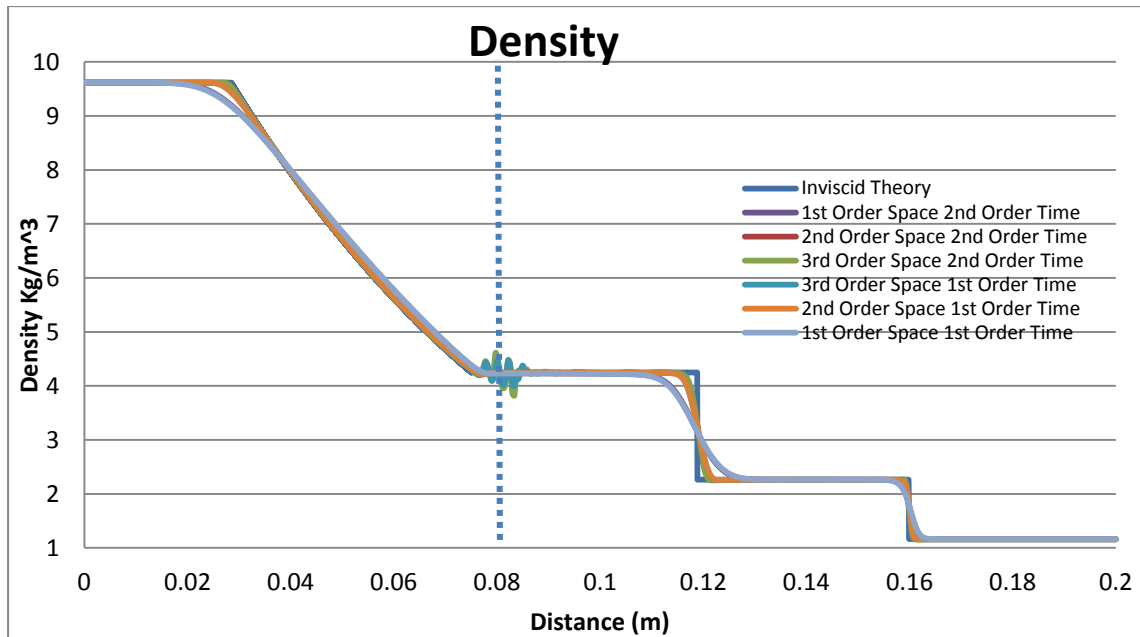
Figure 2. Mi=1.55 Shock Scheme comparison

Problems of this nature often require an adaptive grid to resolve shocks sharply. A comparison of different levels of adaption found that the critical grid size in order to resolve shear layer instabilities is ≈25x25µm. A grid coarser than this fails to resolve instabilities on the shear layer. However, this level of refinement does come at a significant computational cost.

The final simulation used an inviscid, density-based solver which was 2nd order discretised in both space and time. The ASUM+ flux vector splitting scheme was chosen as it is known to perform well when resolving shocks [5]. An initial uniform regular structured grid consisting of quadrilateral 0.4x0.4mm elements was then adapted 4 times per time-step based on the pressure gradient, giving a minimum Δx=25µm. This led to a maximum grid size of 250~300 K cells. An example of the grid is shown in Figure 3. The CFL number was kept at 0.2, as it was found that numbers larger than this gave non-physical oscillations in the region of strong shocks. This very strict CFL criterion suggests that Fluent is a highly non-diffusive code and, if controlled properly, is well suited to problems of this nature.

The simulation took approximately 2 weeks to complete on an Intel core I7 desktop PC with 8GB of RAM running Windows 7 (64 bit). The baseline mesh was generated using Gambit. Post-processing was performed using Tecplot360, allowing for the generation of numerical schlieren and shadowgraph for comparison with experimental results.
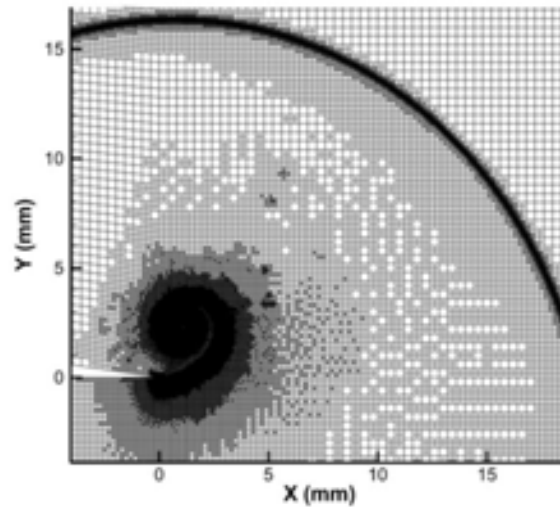
Figure 3. Example grid showing 4 levels of adaption

Experimental Setup

The experiments shown here were carried out in the University of Manchester Aero-Physics Laboratory using the square shock tube. This mechanical rupture style shock tube has a 24.8x24.8mm cross section square tube with a 700mm driver section and a 1700mm driven section. The height of the test section is 55.2mm. A schematic of the test section, which is made of 10mm Perspex, is shown in Figure 4. The geometry tested had a knife- edge tip and a wedge angle of 8°. Driver section pressure measurements and acquisition triggering were performed using two Kulite XT-190M transducers connected to a NI USB-6251 16 bit M series Multifunction DAQ operated by LabView 2011. A Kulite was placed flush to the driven section wall, 1m from the test section. This transducer was connected to an amplifier, hardware delay generator and finally a signal generator to trigger the acquisition.
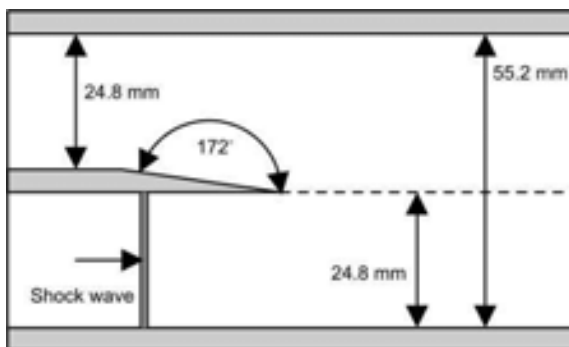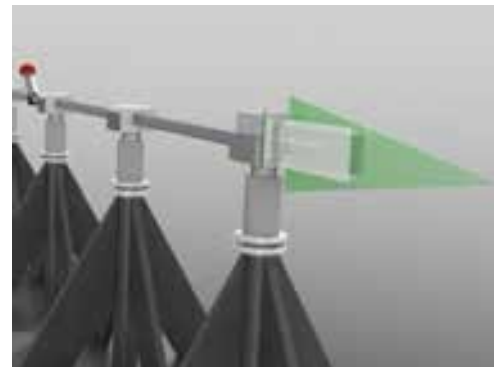

Figure 4. Schematic of test section

Figure 5. Illustration of the shock tube with the PIV laser sheet

Schlieren

Density-based optical measurements were made using a Z-style Toepler schlieren system with a removable knife-edge in order to convert to shadowgraph if required. Continuous illumination came from an in-house constructed, 300W Xenon short arc lamp. Collimated light produced by this lamp was condensed by a hemispherical lens to the slit. Two 8 inch, f=4.5 parabolic mirrors at 3° inclination directed the beam in the standard Z-style to a combination of +1 and +2 diopter macro lenses which focused the beam sharply on the

imaging device. Images were recorded using the Shimadzu HPV-1 at 250Kfps with an exposure time of 2μs. The full-field image shows an area of 67.5 x 56.3 mm while the close-up images show 40.8 x 34.0 mm.

The images recorded were processed using ImageJ. All of the images recorded were divided by a reference image (before the arrival of the shock) in order to remove non-uniform illumination and artifacts on the windows. The image histograms were then scaled to make the flow features more visible. This does have the effect of introducing bright areas around dark regions, although this is easily visible in the images and does not detract from the results.

The experimental shock speed was calculated by taking a slice from each image in the video recorded and stacking them up. This process, known as reslicing, creates an effective x-t diagram where both the distance and time scales are known. The x-t diagram can only be used if the shock wave is planar. Abate and Shyy described this as a *critical* shock [9].

Particle Image Velocimetry

Particle image velocimetry has been applied to problems relating to shock wave diffraction, such as compressible vortex ring propagation [10], but there have been limited applications on moving shock wave interactions. This is primarily due to the available laser repletion rate. This means that any PIV experiments have to be performed in a *spark* fashion, i.e. only acquiring one pair of images per run and then increasing the delay time. Using PIV in this fashion is extremely difficult and time-consuming, as the flow needs to be seeded every run and only one set of data can be extracted.

The PIV system used here consists of the LaVision FlowMaster with an Imager pro X 2M camera and a Litron Nano-L-200-15 PIV Nd:YAG laser. This system allows a very small δt between images, one of the limiting factors in previous studies [11]. For this experiment, $\delta t = 0.55\mu s$. The laser sheet was aimed vertically down the shock tube centreline (see Figure 5), with the camera normal to the laser sheet. Al_2O_3 nanoparticles were injected into the test section using a SciTech Consultants PS-10 powder seeder. The average particle size was estimated to be 0.5μm. The relaxation time was estimated to be 3.6μs using the theory given by Melling [12], with a correction for slip factor and mean free path length. Solid nanoparticles are currently the best particles for use in a flow of this type, where relaxation length and time are the most important factors for credible results. The interrogation window size was 32 x 32 pixels. Raw PIV images were used for laser sheet visualisation, as they highlighted some flow characteristics that were ambiguous in other tests**.**

Results

This section will present the results of each experiment and compare them to the numerical simulations performed.

Numerical Simulations

As mentioned previously, the numerical simulations performed showed a strong grid dependency, especially in the region of the shear layer. As can be seen in Figure 6, the shear layer, expansion fans and the contact are all poorly resolved without strong grid adaption. It should be noted that all the numerical schlieren presented in this section is non-directional. Experiments were performed using a horizontal knife-edge, giving measurements in the vertical direction. If the numerical schlieren image is calculated, based on the y density gradient, normal shock waves are invisible due to the effective zero exposure time. Therefore, for the ease of understanding, density gradient magnitudes are presented (this is akin to a small circular cut-off instead of a knife-edge).

Figure 7 shows numerical schlieren at six of the time steps that were captured experimentally. Figure 7 a) and b) show the beginning of the diffraction process and show the large scale features expected. The reflected sound wave and the contact surface are both clearly resolved, and there appears to be an expansion fan at the apex of the knife-edge geometry. The reflected sound wave propagates upstream (below the knife-edge) at a slower speed than the diffracted shock (above the knife-edge), due to the velocity induced by the incident shock wave. However, it is not clear what is happening around the shear layer due to the strong gradients nearby. At 56μs after impact (Figure 7 c), the shear layer is clearly unstable and is exhibiting the initial stages of the Kelvin-

Helmholtz instability. The instability can first be seen at 40μs after the impact of the shock wave. In the subsequent figures, the diffracted shock wave can be seen reflecting off the upper wall of the test section and propagating back towards the vortex. During this time the velocity induced by the vortex has the effect of slowing the shock wave and causing it to deviate from the regular curvature it exhibits in the early part of the process. It is interesting to note that the train of shocks and expansion fans that are expected on the underside of the shear layer are underpredicted in the simulations. The initial two lambda structures can be seen, but subsequent structures are not resolved [1, 13]. This is likely to be due to the dynamic adaption of the grid as tests on uniform grids (albeit coarser) have been shown to resolve these features successfully.
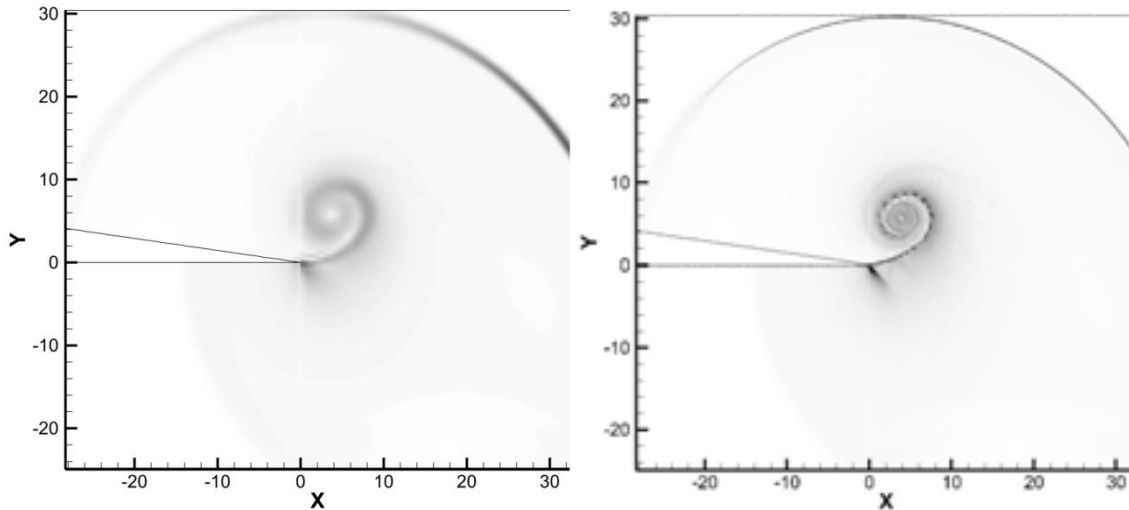

Figure 6.Comparison of baseline (left) and refined (right) mesh at the same time step

Figure 8 shows the numerical velocity vector plots at the corresponding time steps to Figure 7. The velocity vectors have been interpolated on to a uniform grid with the same resolution as the PIV system described previously. This gives 400 x 300 individual velocity vectors. The diffracting shock wave shape can clearly be seen in Figure 8 a-d). As expected, the shock wave is a different strength along all of its curvature, meaning that the induced velocity is lower at larger angles of diffraction (as the shock tends towards a sound wave). As the diffracted shock reflects off the upper surface, it begins to stagnate the flow and deflect it outwards. This leads to the reflecting shock front being visible in the velocity vector plots. The velocity vector plots show the influence of the expansion around the corner clearly as the flow is accelerated to a maximum value of 531 m/s in Figure 8 f). However, this value is localised to one cell, and the expansion region has a larger region of flow with a velocity of 480~490 m/s. It is extremely difficult to discern any instabilities along the shear layer at this resolution.
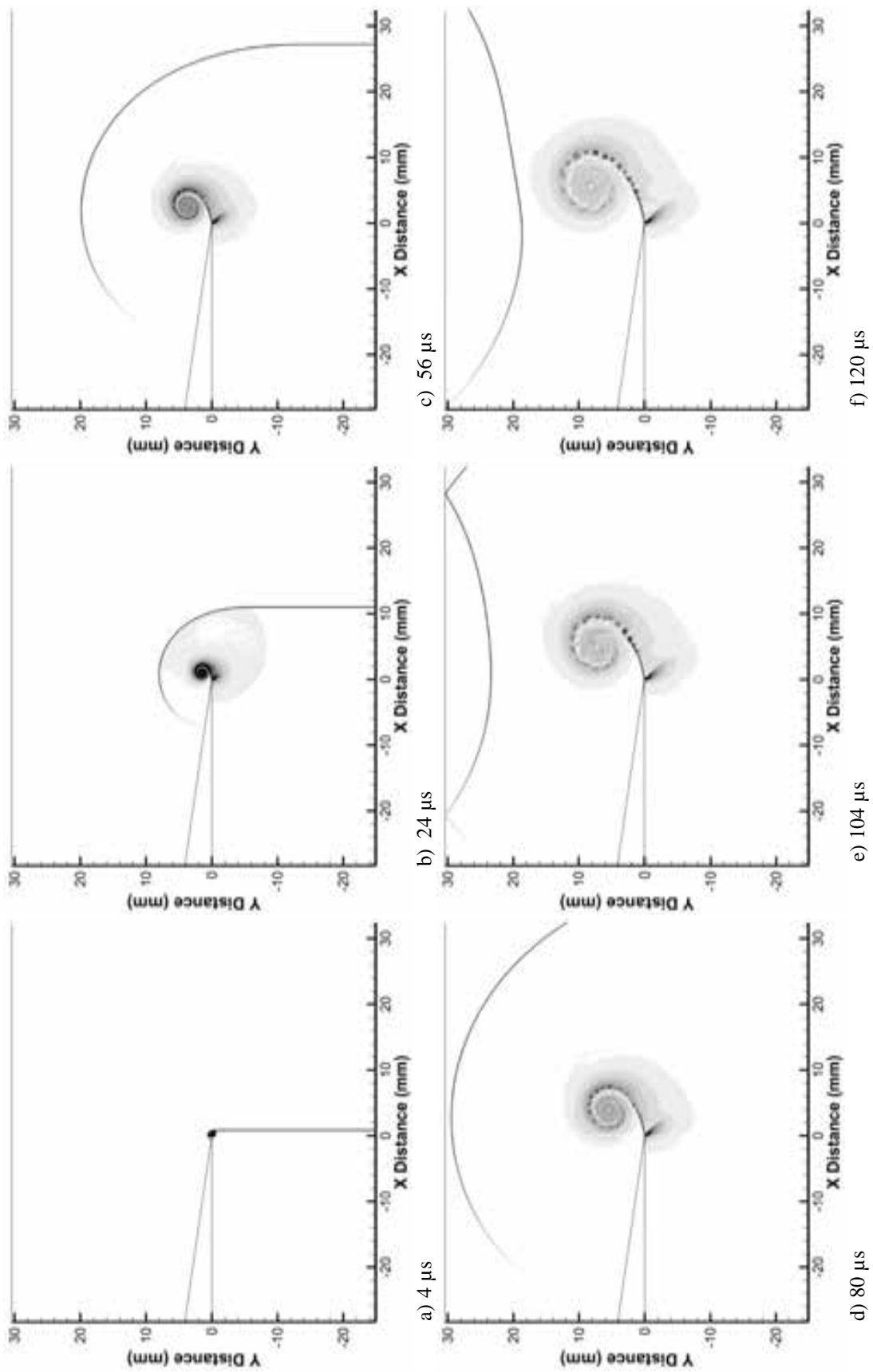
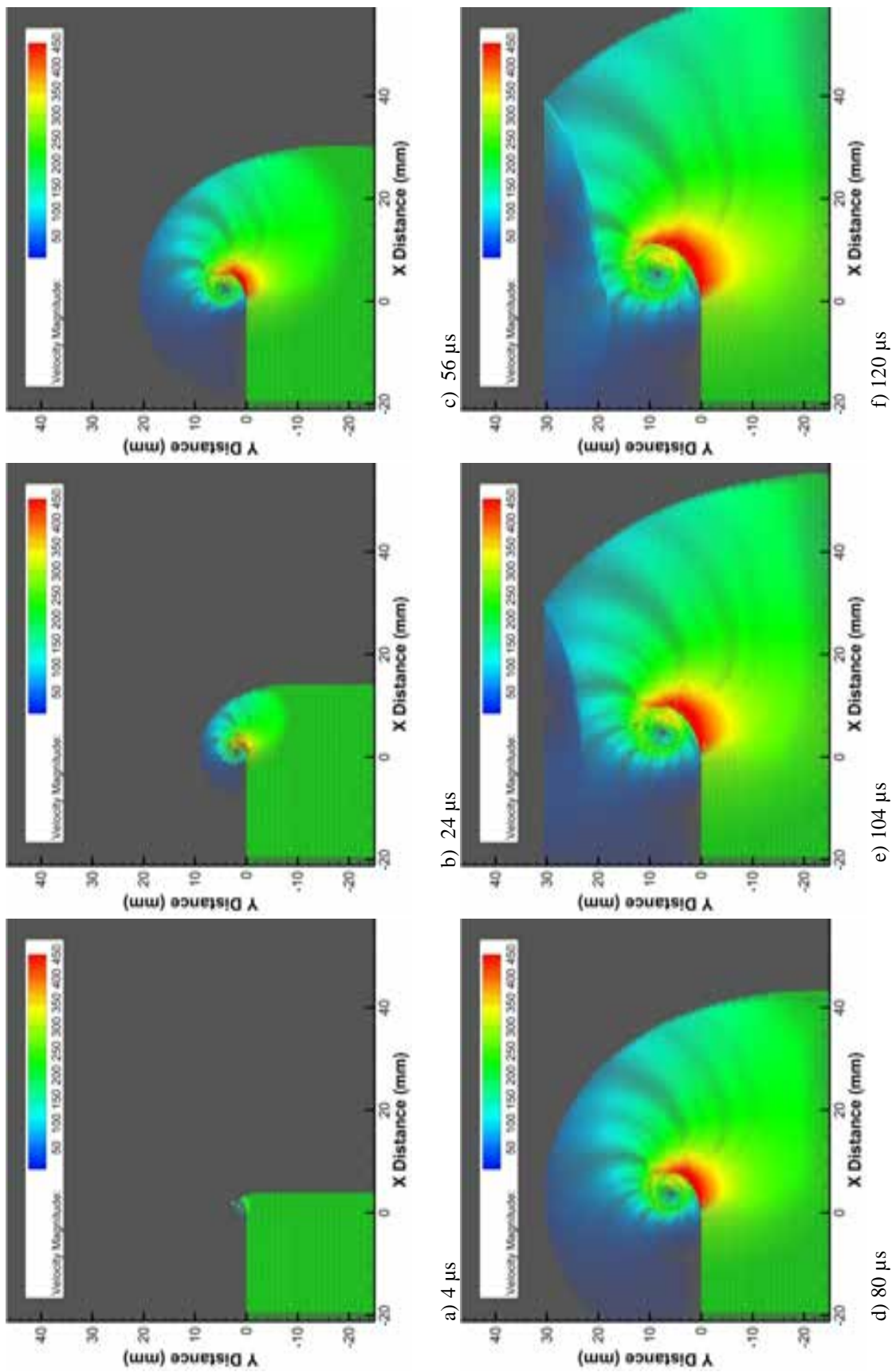**Figure 7. Simulated density gradient magnitude plots at different time steps**

a) 4 μs

b) 24 μs

c) 56 μs

d) 80 μs

e) 104 μs

f) 120 μs

Figure 8. Simulated velocity vector plots at different time steps

Experimental Schlieren

Figure 9, Figure 10, Figure 11 and Figure 12 show experimental schlieren images of different time steps at two different zooms. The close-up images (Figure 10 and Figure 12) both appear to have more noise on them than the full-field images. This is down to the finite amount of light available during the experiments. As the camera is zoomed in, less light falls on the same chip area, meaning that less of the dynamic range of the camera is utilised. The histograms of the two datasets have been adjusted for ease of understanding and comparison. Even though the incident shock wave is travelling in the x-direction and the schlieren system should only be sensitive to density gradients in the y-direction, the shock is still visible. This is due to the finite exposure time of the high-speed schlieren (2μs). In this time the shock has moved approximately 1mm.

The early stages of the shock diffraction process are shown in Figure 9 and Figure 10. In the full-field images (Figure 9) the density gradients are so strong around the main vortex core that the image is overranged in this area. Despite this, the large-scale features are resolved well. The shock shape, contact surface, reflected sound wave and vortex are clearly visible.

Underneath the shear layer it is difficult to see any flow features due to the overranging present. However, in Figure 10 c, there appears to be a structure of lambda shocks that have been seen by previous researchers [1, 13]. As the flow develops in Figure 11 and Figure 12, overranging becomes less of a problem as the density gradients are spread out, meaning that more features become visible. In both the full-field and close-up images, the lambda structures present underneath the shear layer are visible. In Figure 12 c, five distinct lambda structures can be seen with a further two *intensity changes* which are too small to distinguish clearly. These lambda structures were not resolved by the numerical schlieren but are clearly visible in the experimental results.

It is difficult to see in still images (it is much clearer in the high-speed video), but the shear layer has instabilities on it that can be individually resolved. These are most visible in Figure 11 and Figure 12 c. High-speed video results show that these instabilities are present at times as early as 80μs after the shock wave has begun to diffract. The close-up schlieren images (Figure 10 and Figure 12) show the instabilities more clearly than the full-field images. This is significantly longer than the inviscid simulation predicted. The presence of viscosity in the flow may slow down the formation process of these vortices.

In the final images of Figure 11 and Figure 12, the reflected sound wave and reflected shock wave are both influenced by the presence of the expansion region and the vortex respectively. The effect on the curvature of these waves is comparable with the numerical simulations.

Overranging is almost unavoidable in an experiment such as this one due to the large density gradients present. This makes the instabilities on the shear layer extremely difficult to find experimentally, as they are small changes in density obscured in a flow-field full of large changes in density. A real and practical schlieren system can only have a finite sensitivity over a finite range. As schlieren is only sensitive to the first spatial derivative of density, it is prone to being overranged by strong phenomena. Shadowgraph is sensitive to the double spatial derivative of density, meaning that it is less likely to be overranged and is probably the most suitable density-based technique for a flow of this type. There is a trade-off between sensitivity and blur with shadowgraph which was discussed by Biss et al. [14]. This trade-off means that it is difficult to set the sensitivity of a shadowgraph system to be sufficient to capture these instabilities without compromising the spatial resolution of the system so much that they are unclear. This has been achieved by tuning the circle-of-confusion of the system and the depth-of-field so that a good compromise between blur and sensitivity can be achieved [15].
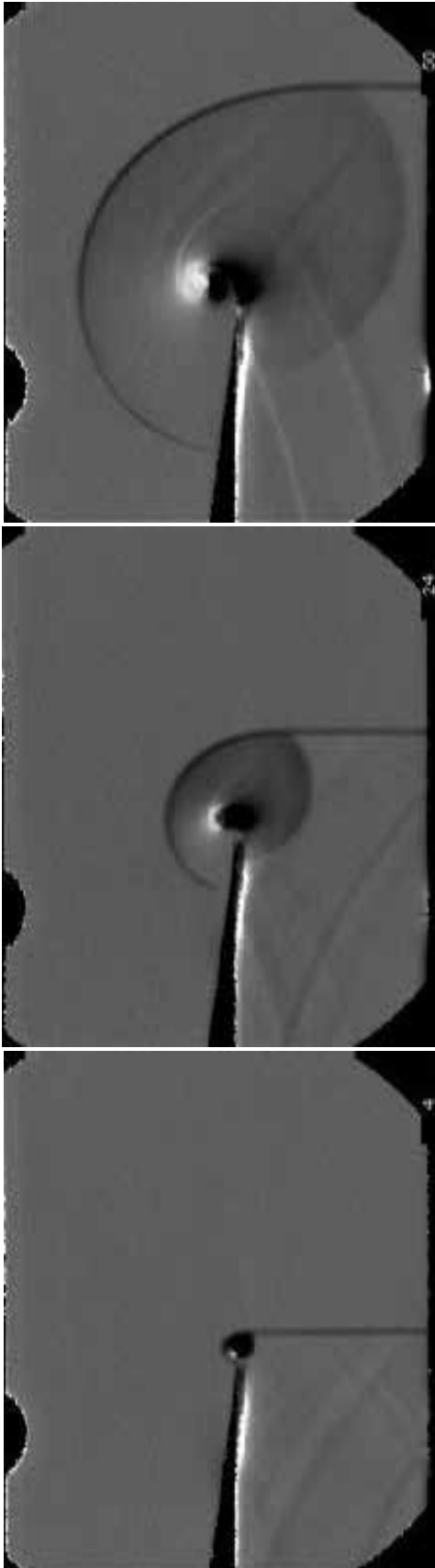
Figure 9. Schlieren montage of full-field images at 4, 24 and 56 μs after shock impingement

Figure 10. Schlieren montage of close-up images at 4, 24 and 56 μs after shock impingement
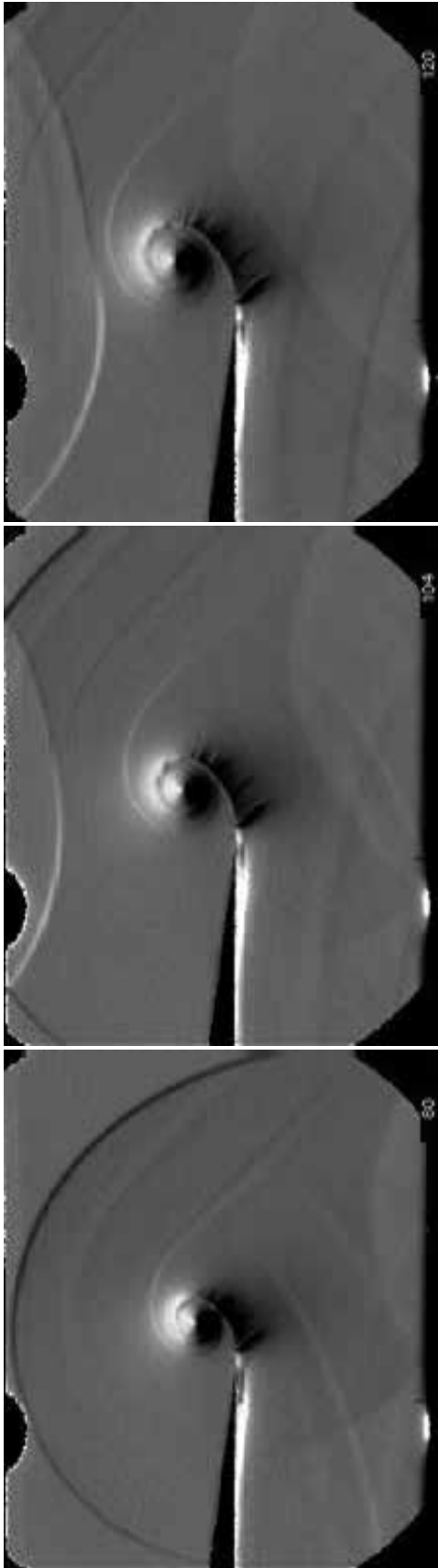
Figure 11. Schlieren montage of full-field images at 80, 104 and 120 μs after shock impingement

Figure 12. Schlieren montage of close-up images at 80, 104 and 120 μs after shock impingement
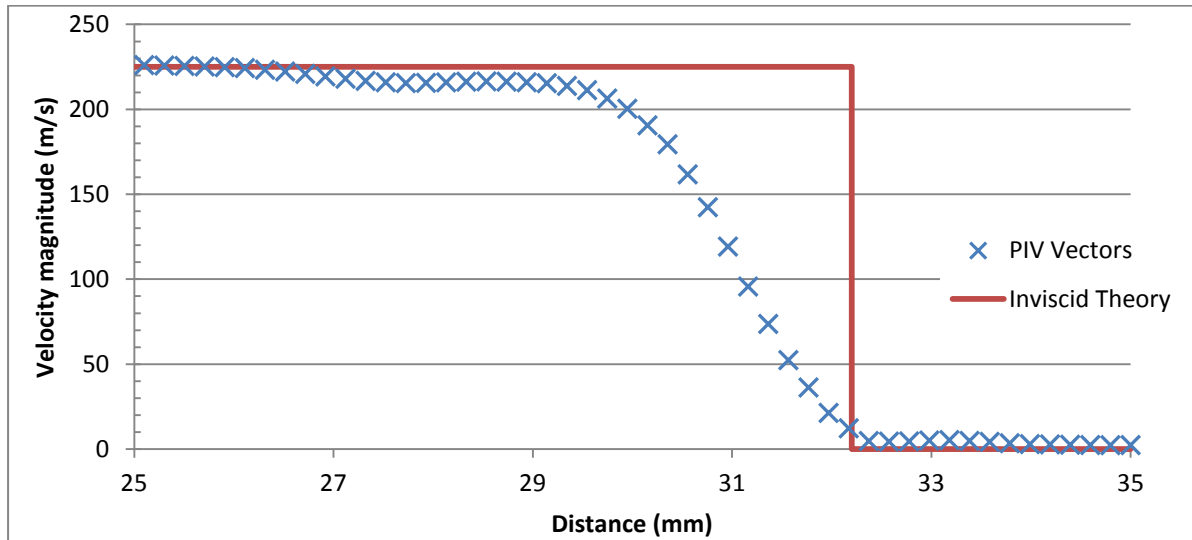
Particle Image Velocimetry

Figure 13. Shock front measurements from PIV

The PIV experiments that were conducted allowed us to use not only the vector map created, but also the raw images as a form of laser sheet visualisation. Achieving uniform seeding in PIV is a challenge in itself, but combining that with a very strong vortex means that there will inevitably be some holes in the vector. The two places where this problem is especially significant are inside the main vortex core and underneath the shear layer in the expansion region. Figure 13 shows the comparison between inviscid theory and PIV measurements of the incident shock wave. The planar incident shock front is resolved by the PIV measurements but is spread across 2.8mm (up to 95% induced velocity). This compares well with the shock spread estimated using Melling's theory [12] modified for moving shock waves, which gives 2.3mm.

The velocity vector plots presented in Figure 14 are a grid of 400x300 vectors at the same resolution as the numerical simulations shown in Figure 8. Despite the challenges mentioned above, there is excellent agreement between the numerical and experimental velocity vector plots. The curvature of the shock front is captured well and the influence of the reflected sound wave is also noticeable, as the flow now has a y-component in that region. The expansion region is shown to be accelerating the flow to supersonic speeds and there is no sign of the effect of the lambda structures seen in the experimental schlieren results. The absolute magnitude of the velocity is approximately 20m/s lower than the simulations in the expansion region. This is to be expected, as PIV will naturally underpredict the magnitude of a change in velocity, whether it be an increase or a decrease. As the diffracted shock wave reflects off the top wall of the test section, the flow is decelerated and begins to spread out, agreeing well with the simulations. The exact location of the reflected shock front is difficult to see in these images due to their small scale, but it is visible at higher zooms. Even if uniform seeding were possible around the vortex region, the grid resolution of the PIV measurements is too low to accurately resolve the instabilities seen on the shear layer.

The raw PIV images can be used as laser sheet visualisation to give a qualitative description of some of the flow features. Figure 15 shows one image from the pair of images used to create the vector plots seen in Figure 14, at each time step. From looking at Figure 15, we can see that the seeding density is not uniform everywhere in the domain. Despite this, there are some seeder particles in regions where there appear to be none, which have allowed the cross correlation algorithm in the PIV software to calculate velocity vectors. The most noticeable thing about these images is how well the shear layer appears to entrain seeder particles. As the nanoparticles have inertia, they are ejected from the vortex core of the main vortex. The particles are also ejected from the vortex cores of the K-H instabilities on the shear layer, creating an outline of them. Figure 15 d, e and f show the outline of the K-H instabilities found on the shear layer. This technique resolves the instabilities more clearly than any other experimental technique.
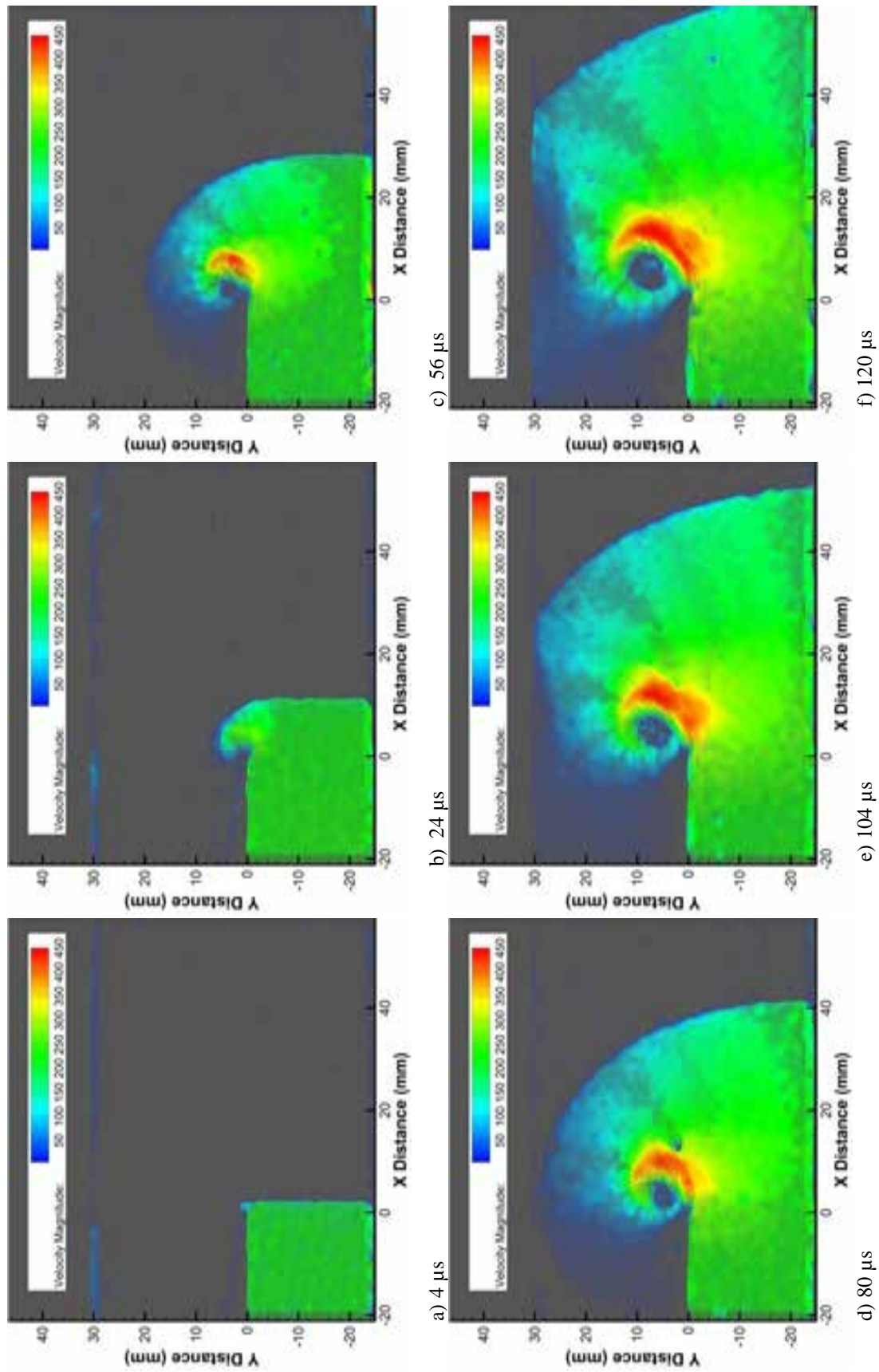
a) 4 μs

b) 24 μs

c) 56 μs

d) 80 μs

e) 104 μs

f) 120 μs

Figure 14. PIV velocity vector plots at different time steps

c) 56 μs

f) 120 μs
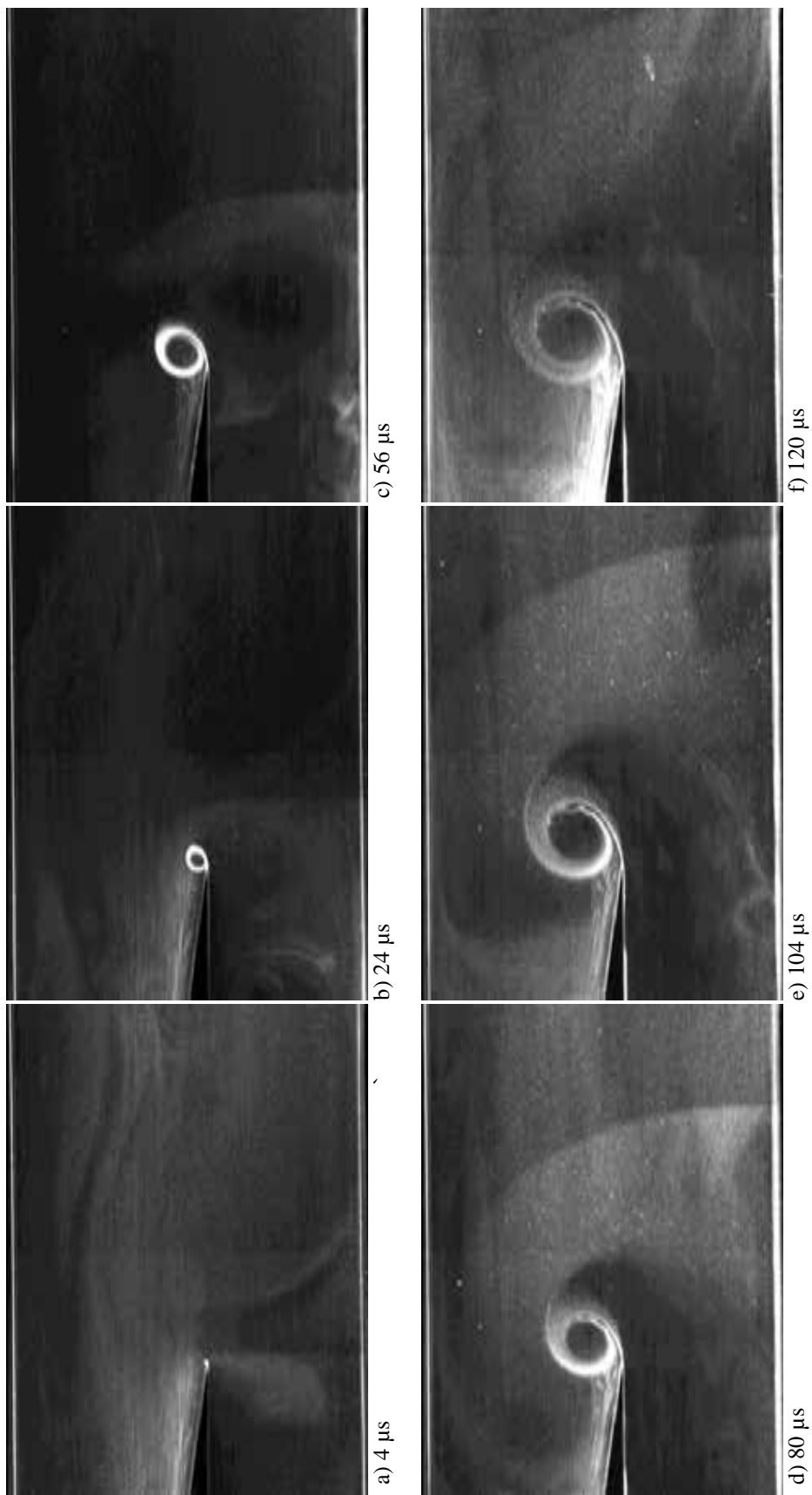
b) 24 μs

e) 104 μs

a) 4 μs

d) 80 μs

Figure 15. Laser sheet visualization from Raw PIV images at different time steps

Conclusion

Shock wave diffraction of a M_i=1.46 shock wave has been investigated using simulations and a variety of experimental techniques. The numerical simulations, performed by a commercial CFD package, show a wide range of flow features. However, some of the flow features were only present if the grid was fine enough to resolve them; in particular, the K-H instabilities on the shear layer. Despite the fine grid resolution, some flow features were underpredicted. The lambda wave structures underneath the shear layer are very poorly resolved in the simulations; this appears to be dependent on the grid adaption scheme used. Numerical schlieren and velocity vector plots have been generated for direct comparison with the experiments performed.

High-speed schlieren measurements have been performed using the Shimadzu HPV-1 camera. These images, taken at a large magnification, provided a good spatial and temporal resolution. Both are essential for a complete understanding of such a transient flow. The experimental schlieren results have shown a large number of lambda wave structures underneath the shear layer which have not been resolved in simulations or using any other experimental technique. The schlieren images (particularly at the highest zoom) appear to show instabilities on the shear layer, but these images are compelling enough evidence to say that all of the flow features are resolved correctly. PIV measurements have been performed in a spark fashion in order to gain velocity vector plots for comparison with CFD. The PIV vectors resolve the shock front adequately but tend to underpredict changes in velocity such as those found in the expansion region under the shear layer. PIV measurements are extremely tricky in the vicinity of strong vortices, as particles are ejected from the vortex core. This is an unavoidable problem, unless one can find particles with zero inertia. However, the inertia characteristics of the particles outline any vortices in the flow-field, and using raw PIV images as laser sheet visualisation allows us to see more convincing evidence of the presence of K-H instabilities on the shear layer.

From this work we can see that CFD can resolved the majority of the flow features (if the grid is fine enough); however, there are some that it fails to resolve. The same is true of schlieren and PIV. When used independently, these techniques give a good understanding of the flow but not a complete picture. When these methods are combined, all of the flow features can be resolved, giving us a complete understanding.

References

[1]   B. W. Skews, "The Perturbed Region Behind a Diffracting Shock Wave," *Journal of Fluid Mechanics,* vol. 29, pp. 705-719, 1967.

[2]   M. Sun and K. Takayama, "Vorticity Production in Shock Diffraction," *Journal of Fluid Mechanics,* vol. 478, pp. 237-256, 2003.

[3]   K. Takayama and Y. Inoue, "Shock Wave Diffraction over a 90 degree Sharp Corner," *Shock Waves,* vol. 1, pp. 301-312, 1991.

[4]   M. Sun and K. Takayama, "A Note on Numerical Simulation of Vortical Structures in Shock Diffraction," *Shock Waves,* vol. 13, pp. 25-32, 2003.

[5]   S. De and M. Thangadurai, "Numerical Simulation of Shock Tube Generated Vortex Effect of Numerics," *International Journal of Computational Fluid Dynamics,* vol. 25, pp. 345-354, 2011.

[6]   T. I. Tseng and R. J. Yang, "Numerical Simulation of Vorticity Production in Shock Diffraction," *AIAA Journal,* vol. 44, pp. 1040-1047, 2006.

[7]   B. W. Skews*, et al.*, "Shear Layer Evolution in shock Wave Diffraction," in *28th International Symposium on Shock Waves*, Manchester, UK, 2011.

[8]   B. Skews*, et al.*, "Shear layer behavior resulting from shock wave diffraction," *Experiments in Fluids,* vol. 52, pp. 417-424, 2012.

[9]   G. Abate and W. Shyy, "Dynamic Structure of Confined Shocks Undergoing Sudden Expansion," *Progress in Aerospaces Sciences,* vol. 38, 2002.

[10]   R. Mariani and K. Kontis, "Experimental studies on coaxial vortex loops," *Physics of Fluids,* vol. 22, p. 126102, 2010.

[11]   M. K. Quinn*, et al.*, "Experimental Studies of Shock Wave Diffraction," in *28th International Symposium on Shock Waves*, Manchester, UK, 2011.

[12]   A. Melling, "Tracer Particles and Seeding for Particle Image Velocimetry," *Measurement Science and Technology,* vol. 8, pp. 1406-1416, 1997.

[13]   M. Sun and K. Takayama, "The Formation of a Secondary Wave Behind a Shock Wave Diffracting at a Convex Corner," *Shock Waves,* vol. 7, pp. 287-295, 1997.

[14]   M. M. Biss*, et al.*, "High-speed digital shadowgraphy of shock waves from explosions and gunshots," in *26th International Symposium on Shock Waves*, Gottingen, Germany, 2007.

[15]   M. K. Quinn and K. Kontis, "Experiments and Simulations of Weak Shock Wave Diffraction Phenomena," presented at the 20th International Shock Interaction Symposium, Stockholm, Sweden, 2012.